Received: 9 March 2021 | Revised: 22 June 2021 | Accepted: 25 June 2021

DOI: 10.1002/jnr.24923

RESEARCH ARTICLE

JOURNAL OF Neuroscience Research

# Sequential MAVS and MyD88/TRIF signaling triggers anti-viral responses of tick-borne encephalitis virus-infected murine astrocytes

Luca Ghita[1] | Veronika Breitkopf[2] | Felix Mulenge[1] | Andreas Pavlou[1,3] | Olivia Luise Gern[1,4] | Verónica Durán[1] | Chittappen Kandiyil Prajeeth[3] | Moritz Kohls[5] | Klaus Jung[5] | Martin Stangel[3,6] | Imke Steffen[2] | Ulrich Kalinke[1,6]

[1]Institute for Experimental Infection Research, TWINCORE, Centre for Experimental and Clinical Infection Research, a joint venture between the Helmholtz Centre for Infection Research and the Hannover Medical School, Hannover, Germany

[2]Institute for Biochemistry and Research Center for Emerging Infections and Zoonoses (RIZ), University of Veterinary Medicine Hannover, Foundation, Hannover, Germany

[3]Clinical Neuroimmunology and Neurochemistry, Department of Neurology, Hannover Medical School, Hannover, Germany

[4]Department of Pathology, University of Veterinary Medicine Hannover, Foundation, Hannover, Germany

[5]Institute for Animal Breeding and Genetics, University of Veterinary Medicine Hannover, Foundation, Hannover, Germany

[6]Cluster of Excellence - Resolving Infection Susceptibility (RESIST, EXC 2155), Hannover Medical School, Hannover, Germany

**Correspondence**
Imke Steffen, Institute for Biochemistry and Research Center for Emerging Infections and Zoonoses (RIZ), University of Veterinary Medicine Hannover, Foundation, Bünteweg 17, 30559 Hannover, Germany.
Email: imke.steffen@tiho-hannover.de

Ulrich Kalinke, Institute for Experimental Infection Research, TWINCORE, Centre for Experimental and Clinical Infection Research, Feodor-Lynen-Str. 7, 30625 Hannover, Germany.
Email: ulrich.kalinke@twincore.de

**Present address**
Luca Ghita, Department of Medicine, Division of Infectious Disease and Geographical Medicine, Stanford University School of Medicine, Stanford, CA, USA and Luca Ghita, Department of Microbiology and Immunology, Stanford University School of Medicine, Stanford, CA, USA
Chittappen Kandiyil Prajeeth, Research Center for Emerging Infections and Zoonoses, University of Veterinary Medicine Hannover, Foundation, Hannover, Germany

## Abstract

Tick-borne encephalitis virus (TBEV), a member of the *Flaviviridae* family, is typically transmitted upon tick bite and can cause meningitis and encephalitis in humans. In TBEV-infected mice, mitochondrial antiviral-signaling protein (MAVS), the downstream adaptor of retinoic acid-inducible gene-I (RIG-I)-like receptor (RLR) signaling, is needed to induce early type I interferon (IFN) responses and to confer protection. To characterize the brain-resident cell subset that produces protective IFN-β in TBEV-infected mice, we isolated neurons, astrocytes, and microglia from mice and exposed these cell types to TBEV in vitro. Under such conditions, neurons showed the highest percentage of infected cells, whereas astrocytes and microglia were infected to a lesser extent. In the supernatant (SN) of infected neurons, IFN-β was not detectable, while infected astrocytes showed high and microglia low IFN-β expression. Transcriptome analyses of astrocytes implied that MAVS signaling was needed early after TBEV infection. Accordingly, MAVS-deficient astrocytes showed enhanced TBEV infection and significantly reduced early IFN-β responses. Nevertheless, at later time points, moderate amounts of IFN-β were detected in the SN of infected MAVS-deficient astrocytes. Transcriptome analyses indicated that MAVS deficiency negatively affected

**Abbreviations:** CNS, central nervous system; DEGs, differentially expressed genes; DENV, dengue virus; hpi, hours post-infection; IFN, interferon; ISGs, interferon-stimulated genes; JEV, Japanese encephalitis virus; LGTV, Langat virus; MAVS, mitochondrial antiviral-signaling protein; MyD88, myeloid differentiation primary response 88; PRRs, pattern recognition receptors; RABV, rabies virus; RLRs, retinoid acid-inducible gene-I (RIG-I)-like receptors; TBEV, tick-borne encephalitis virus; TLR, Toll-like receptors; TRIF, TIR-domain-containing adaptor-inducing interferon-ß; WNV, West Nile virus; WT, wild type; ZIKV, Zika virus.

Edited by Bradley Kerr, David McArthur, and Cristina Ghiani. Reviewed by Daniel Ruzek and Stipan Jonjic.

**Funding information**
This study was funded by the Deutsche Forschungsgemeinschaft (DFG; German Research Foundation)—398066876/GRK 2485/1 to K.J., I.S., and U.K.; the Deutsche Forschungsgemeinschaft (DFG; German Research Foundation)—158989968—SFB 900-B2 to U.K.; the Deutsche Forschungsgemeinschaft (DFG; German Research Foundation) under Germany's Excellence Strategy—EXC 2155 "RESIST"—Project ID 39087428 to M.S. and U.K.; by the Federal Ministry of Education and Research (BMBF) under project number 01KI1719 as part of the Research Network Zoonotic Infectious Diseases to I.S.; the Niedersachsen-Research Network on Neuroinfectiology (N-RENNT) of the Ministry of Science and Culture of Lower Saxony, Germany, to M.S. and U.K., and by the Helmholtz Association (Zukunftsthema "Immunology & Inflammation" (ZT-0027)) to U.K..

the induction of early anti-viral responses, which resulted in significantly increased TBEV replication. Treatment with MyD88 and TRIF inhibiting peptides reduced only late IFN-β responses of TBEV-infected WT astrocytes and blocked entirely IFN-β responses of infected MAVS-deficient astrocytes. Thus, upon TBEV exposure of brain-resident cells, astrocytes are important IFN-β producers showing biphasic IFN-β induction that initially depends on MAVS and later on MyD88/TRIF signaling.

**KEYWORDS**
astrocytic anti-viral response, flaviviruses, innate immunity, MAVS signaling, neurotropic infection, tick-borne encephalitis virus

## 1 | INTRODUCTION

Tick-borne encephalitis virus (TBEV) is a neurotropic positive-strand RNA virus belonging to the *Flaviviridae* family, genus *Flavivirus*. This virus is closely related to other flaviviruses such as West Nile virus (WNV), Japanese encephalitis virus (JEV), dengue virus (DENV), and others (Kuno et al., 1998). TBEV is a constantly spreading zoonotic pathogen in Europe and Asia. The virus is transmitted via tick bites or consumption of infected milk (Dumpis et al., 1999; Kerbo et al., 2005). Between 2012 and 2016, a total of 12,500 cases of TBEV infection were reported in Europe (Beaute et al., 2018) and more recently this number increased up to 13,000 per year worldwide (Lindquist & Vapalahti, 2008). Mostly, TBEV infection is associated with moderate disease, whereas in 10% of the cases a severe disease course is observed that culminates in the development of neurological syndromes such as encephalitis, meningitis, and paralysis (Gritsun et al., 2003; Heinz & Kunz, 2004; Lindquist & Vapalahti, 2008; Mansfield et al., 2009). The mortality rate ranges between 0.5% and 30%, depending on the virus strain. Thirty to 60% of patients who recovered from TBEV-induced encephalitis develop neurological sequelae (Gritsun et al., 2003; Heinz & Kunz, 2004; Lindquist & Vapalahti, 2008; Mansfield et al., 2009). The increasing numbers of cases of TBEV-induced encephalitis and the expansion of TBEV-affected areas in Europe highlight the medical relevance of TBEV. A vaccine is available, however, it is often not recommended outside of known endemic areas (Hellenbrand et al., 2019). Treatment options are not causative and limited to supportive care. This is due to the limited understanding of TBEV pathogenesis and immunity (Lani et al., 2014).

Upon bites by TBEV-infected ticks, the virus is able to reach the central nervous system (CNS). While, multiple CNS entry routes have been described for flaviviruses (Koyuncu et al., 2013), TBEV was shown to gain access by direct infection of brain microvascular endothelial cells (Palus et al., 2017). Within the CNS, TBEV productively infects neurons and astrocytes, which leads to the development of neuropathology (Bílý et al., 2015; Palus et al., 2014; Růžek et al., 2009). CNS-resident cells are able to sense virus RNA through pattern recognition receptors (PRRs) and then mount anti-viral responses (Goubau et al., 2013). The PRRs mainly involved in the sensing of RNA viruses include the endosomal Toll-like receptors (TLRs) and the cytoplasmic retinoid acid-inducible gene-I (RIG-I)-like receptors (RLRs) (Carty et al., 2014; Goubau et al., 2013; Kawai & Akira, 2011). While TLRs are differentially expressed on CNS-resident cell types, RLRs were shown to be ubiquitously expressed (Furr et al., 2008; McCarthy et al., 2017; Trudler et al., 2010). Upon sensing of virus RNA within the cytosol, RLRs including RIG-I, LGP2, and MDA5 trigger downstream signaling through the adaptor

### Significance

Tick-borne encephalitis virus (TBEV) is a zoonotic pathogen constantly spreading in Europe and Asia. TBEV is mostly transmitted by the bite of infected ticks and the infection can result in the development of encephalitis. Although an approved vaccine is available, due to the poor understating of disease pathogenesis treatment options are limited and ineffective. Here we uncovered that upon TBEV infection of brain-resident cells, astrocytes are important IFN-β producers, thus contributing to innate anti-viral responses. Moreover, we found that IFN-β induction in astrocytes by TBEV infection has a biphasic kinetics that initially depends on MAVS and later on MyD88/TRIF signaling.

molecule mitochondrial anti-viral signaling protein (MAVS) (Hou et al., 2011). Triggering of MAVS induces activation of the transcription factors IRF3 and NF-κB, which leads to the induction of protective type I interferon (IFN) responses and expression of anti-viral genes (Sharma et al., 2003).

Studies on TBEV pathogenesis revealed a crucial role of RLR signaling in the initiation of anti-viral immune responses. Upon infection with TBEV or Langat virus (LGTV), a low-virulent relative of TBEV, MAVS-deficient mice (MAVS ko) showed enhanced susceptibility to lethal infection (Kurhade et al., 2016). Moreover, it was shown that LGTV infected MAVS ko animals presented with enhanced viral loads in the CNS. The lack of the MAVS adaptor molecule was correlated with an increased LGTV replication within neurons and astrocytes (Kurhade et al., 2016). Recently, it became evident that astrocytes actively participate in generating protective immunity upon TBEV infection. Cytokines and chemokines were shown to be released from astrocytes, thus contributing to the induction of an anti-viral state (Lindqvist et al., 2016; Pokorna Formanova et al., 2019). Nonetheless, the astrocytic intrinsic mechanisms that initiate anti-viral responses upon TBEV infection are not well understood. Here we showed that murine neurons, astrocytes, and microglia are productively infected upon in vitro exposure to TBEV, whereas astrocytes are the main producers of IFN-β protein. Transcriptome analyses revealed that the mechanisms underlying astrocytic responses to TBEV were strictly dependent on MAVS signaling at early stages of infection, as MAVS ko astrocytes showed increased infection and reduced IFN-β production. Nevertheless, at later stages of infection, MAVS ko astrocytes mounted moderate IFN-β responses indicating the contribution of a MAVS-independent mechanism, which turned out to be dependent on MyD88/TRIF signaling.

## 2 | MATERIALS AND METHODS

### 2.1 | Virus propagation and quantification

TBEV strain Neudoerfl (GenBank accession number U27495) was originally isolated from a tick in Austria in 1971 (Mandl et al., 1989). The virus is a gift from the collection of the Department of Microbiology of the German Armed Forces in Munich, Germany and was passaged twice in A549 cells (RRID:CVCL_0023) by infection at MOI 0.01 in high-glucose Dulbecco's modified Eagle's medium (DMEM) supplemented with penicillin (10,000 U/ml), streptomycin (10 mg/ml), and L-glutamine (200 mM) (Sigma). After 1 hr of incubation, the inoculum was removed and exchanged by DMEM supplemented with 2% fetal calf serum (FCS), penicillin and streptomycin, and L-glutamine. The supernatant was collected after 5 days and virus titration was performed on A549 cells (RRID:CVCL_0023). Viral RNA was extracted from culture supernatants with Qiagen Viral RNA Mini Kit and quantification of genome copies was performed by probe-based quantitative RT-PCR as previously described (Schwaiger & Cassinotti, 2003).

### 2.2 | Mice

C57BL/6 (Wild type or WT, Envigo, RRID:IMSR_JAX:000664) and B6.STOCK-Mavs(tm1Tsc) (MAVS ko, RRID:MGI:3802510) (Michallet et al., 2008) mice were bred under specific pathogen-free conditions in the central mouse facility of the Helmholtz Centre for Infection Research, Brunswick, and at TWINCORE, Centre for Experimental and Clinical Infection Research, Hanover, Germany. Mouse experimental work was carried out in compliance with regulations of the German Animal Welfare Law.

### 2.3 | Murine primary CNS-resident cell isolation and culturing

Mice were euthanized by cervical dislocation and embryos extracted under sterile conditions. Neurons were isolated and cultivated from mouse embryos at embryonic day 12.5. For each preparation, a total of five to seven embryos were used. The cortex was freed of meninges and dissected on ice-cold PBS using a stereomicroscope (Nikon, SMZ45T), then it was collected in ice-cold Hanks Balanced Salt Solution (HBSS, Gibco) and minced using fine dissection scissors. Next, the minced tissue was incubated in 500 µl of trypsin-EDTA (Biochrome) and 2 µl of DNase (Roche) for 8 min at 37°C. Four milliliter of DMEM medium (Gibco) was then added and mechanical dissociation with a 1 ml pipet was performed. The solution containing the dissociated cortex was then resuspended in 2 ml of neurobasal complete medium (Gibco) containing media supplements (1x B-27, Gibco; 1x N2, Gibco; 1% Pen/Strep, Capricorn; 1% GlutaMax, Gibco) and neurons were seeded in poly-L-lysine (Sigma) coated 24-well plates or on poly-L-lysine coated glass coverslips at a density of $2.5 \times 10^5$ cells per well. Cells were cultured in neurobasal complete medium (1x B-27, Gibco; 1x N2, Gibco; 1% Pen/Strep, Capricorn; 1% GlutaMax, Gibco) at 37°C in 5% $CO_2$. Neuronal purity was between 72% and 80% as determined by immunocytochemistry and microscopy. Cells were immunolabeled with NeuN and DAPI and the ratio of NeuN and DAPI double-positive cells and the total number of DAPI positive cells was used to determine the purity of neuronal culture, which was between 72% and 80%. Neurons were kept in culture for 7 days before infection and fresh neurobasal complete medium was added every second day.

Microglia and astrocytes were isolated as previously described (Prajeeth et al., 2018). In brief, six to eight newborn mice for each cell isolation procedure were decapitated at day 3 post-birth, brains were dissected and meninges and blood vessels were removed using a stereomicroscope (Nikon, SMZ45T). Next, the brains were minced and digested with 0.1% trypsin (Sigma-Aldrich) and 0.25% DNAse (Roche), single cell suspensions were seeded in precoated poly-L-lysine flasks in DMEM with 1% penicillin/streptomycin (Gibco) supplemented with 10% FCS and cultivated at 37°C in 5% $CO_2$. Medium was changed on day 1 and subsequently every 3 days. Microglia were collected after 9–11 days of culturing followed by shaking the flasks at 37°C (180 rpm) in an orbital shaker for 40 min. Microglia was collected from the SN

and plated at a density of $2.5 \times 10^5$ cells per well into a 24-well plate or on glass coverslips and kept at 37°C in 5% $CO_2$. Microglia were used the following day for experiments. Microglia purity was between 94% and 97% as determined by flow cytometry (Prajeeth et al., 2018). Astrocytes were isolated after removing remaining microglia and oligodendrocytes by over-night shaking at 37°C (170 rpm), followed by cytosine β-D-arabinofuranoside (AraC, Sigma-Aldrich) treatment for 3 days at 37°C in 5% $CO_2$. Astrocytes were detached by trypsin-EDTA (bio-sell) treatment and plated into a 24-well plate or on glass coverslips at a density of $2.5 \times 10^5$ cells per well and kept at 37°C in 5% $CO_2$. Medium was changed 24 hr after seeding and then the cells were used for infection experiments. Astrocytes purity was 95 to 98% as determined by flow cytometry (Prajeeth et al., 2018).

## 2.4 | Infection and treatment of CNS primary cells

All cell types were inoculated at a MOI of 1 of TBEV in serum- and antibiotic free DMEM medium for 1 hr at 37°C in 5% $CO_2$, then washed with warm PBS and incubated with the respective culture medium at 37°C in 5% $CO_2$. MyD88 and TRIF inhibition experiments were performed by pre-treating astrocytes with 5 μM of Pepinh-MYD and Pepinh-TRIF (Invivogen) for 8 hr. At 12 and 24 hr post-infection, cell-free SN was collected and stored at −80°C for IFN-β analysis and TBEV copy number determination. For RNA analyses, the adhering cells were then harvested, lysed by TRIzol (Thermo Fischer) and stored at −80°C.

## 2.5 | Immunocytochemistry and microscopy

Coverslips were fixed in 4% paraformaldehyde for 20 min at RT, then washed and stored in PBS. Non-specific binding of antibodies was inhibited by incubation for 1 hr at room temperature with blocking buffer containing 3% donkey serum (Sigma-Aldrich) and 0.3% Triton (Sigma-Aldrich) in PBS. Then, the primary antibodies in blocking buffer were added for 2 hr at 4°C. Excess antibodies were removed through three washing steps with PBS before incubation for 1 hr at room temperature with the secondary antibodies in blocking buffer. After washing, nuclei were counterstained with DAPI (4′,6-diamino-2-phenylindole, 1:10.000, Thermo Fisher Scientific, RRID:AB_2307445) and the coverslips were mounted with mounting medium (DAKO) on glass slides. Pictures were taken on a Leica microscope SP8 using LAS-X software and analyzed by Fiji (RRID:SCR_002285). Primary antibodies: rabbit anti-mouse β-III tubulin (Tuj1) (Biolegend; 1:400; RRID:AB_2313773), rabbit anti-mouse GFAP (Millipore; 1:400, RRID:AB_2109645), rabbit anti-mouse Iba-1 (Wako; 1:200, RRID:AB_839506), and mouse anti-dsRNA (J2, Scicons English and Scientific Consulting, TBEV replication foci; 1:500, RRID:AB_2651015). Secondary antibodies: donkey anti-rabbit AF555 (Invitrogen; 1:500, RRID:AB_162543), donkey anti-mouse AF594 (Invitrogen; 1:500, RRID:AB_141633), and donkey anti-mouse AF 647 (Invitrogen; 1:500, RRID:AB_162542) (Table 1).

## 2.6 | IFN-β analysis

IFN-β protein levels were determined from cell-free SNs of mock-treated and TBEV-infected cells, using the VeriKine Mouse Interferon ELISA kit (PBL Assay Science, RRID:SCR_006852) and VeriKine Mouse Interferon ELISA High Sensitivity kit (PBL Assay Science, RRID:SCR_006852) according to the manufacturer's handbook.

## 2.7 | Determination of viral titers by TCID50

Quantification of infectious viral particles from SNs of infected astrocytes was performed by Medium Tissue Culture Infectious Dose

**TABLE 1** Antibody information

| Name | Supplier ID | RRID | Immunogen, host | Dilution |
|---|---|---|---|---|
| Tuj1 | BioLegend; Cat# 801201 | RRID:AB_2313773 | Purified anti-Tubulin beta 3 (TUBB3) antibody, Mouse monoclonal | 1:400; IF |
| GFAP | Millipore; Cat# AB5804 | RRID:AB_2109645 | Anti-Glial Fibrillary Acidic Protein (GFAP) antibody, Rabbit polyclonal | 1:400; IF |
| Iba-1 | FUJIFILM Wako Shibayagi; Cat# 016–20001 | RRID:AB_839506 | Anti-Iba1 antibody, Rabbit monoclonal | 1:200; IF |
| dsRNA | SCICONS; Cat# 10010200 | RRID:AB_2651015 | J2 monoclonal antibody (mAb), Mouse monoclinal | 1:500; IF |
| Donkey IgG AF555 | Thermo Fisher Scientific; Cat# A-31572 | RRID:AB_162543 | Donkey anti-Rabbit IgG (H + L), Polyclonal, Alexa Fluor 555 | 1:500; IF |
| Donkey IgG AF594 | Thermo Fisher Scientific Cat# A-21203 | RRID:AB_141633 | Donkey anti-Mouse IgG (H + L), Polyclonal, Alexa Fluor 594 | 1:500; IF |
| Donkey IgG AF647 | Thermo Fisher Scientific Cat# A-31571 | RRID:AB_162542 | Donkey anti-Mouse IgG (H + L), Policlonal, Alexa Fluor 647 | 1:500; IF |
| DAPI | Thermo Fisher Scientific Cat# D3571 | RRID:AB_2307445 | DNA dye | 1:10,000; IF |

(TCID50) method as previously described (Reed & Muench, 1938). Briefly, SNs of infected primary astrocytes were collected and stored at −80°C, SNs were thawed and 10-fold serial dilutions were transferred onto a monolayer of BHK-21 cells (RRID:CVCL_1915). At 5 days post-infection, the cytopathic effect of virus replication was analyzed by microscopy and the TCID50 value as well as the corresponding plaque forming units per milliliter (PFU/ml) was calculated using the method by Reed and Muench (1938).

### 2.8 | RNA isolation and sequencing

RNA was isolated from WT and MAVS ko astrocytes that were either untreated or TBEV-infected for 12 or 24 hr. RNA was extracted using Direct-zol RNA Miniprep Plus Kit (Zymo Research) according to the manufacturer's instructions. RNA quality and integrity were assessed with Bioanalyzer 2100 (Agilent) and samples with RIN value >8.0 were selected for further processing. Sequencing libraries were constructed and processed on Illumina NovaSeq-600 platform with 50 bp paired-end read configuration. Quality control of the sequenced raw FASTQ files was performed with FastQC software (version 0.11.9) and mapped to Ensembl mouse genome reference version GRCm38 (mm10) using STAR (Dobin et al., 2013) (version 2.5.4b). Gene abundance was also determined by STAR, and differential expression analysis was performed with the DESeq2 package (Love et al., 2014) in the R environment (RRID:SCR_000432), setting the FDR to 0.05. Functional annotation and enrichment analysis was performed, as previously described (Beissbarth & Speed, 2004), on the sets of differentially regulated genes using the Gene Ontology and Reactome databases.

### 2.9 | Statistical analysis

Data are represented as mean ± standard deviation (*SD*). Statistical analysis was performed with GraphPad Prism Version 9.0a (RRID:SCR_002798) for Mac OS X adopting unpaired *Student's t* test, two-tailed Mann–Whitney U test, one-way ANOVA with Tukey's multiple comparison test or ordinary two-way ANOVA with Sidak's multiple comparisons test; ns = not significant ($p > 0.05$), $^{*}p < 0.05$; $^{**}p < 0.01$; $^{***}p < 0.001$; $^{****}p < 0.0001$. RNA-seq data analysis and the principal component analysis were performed with the statistical software RStudio (RRID:SCR_000432).

## 3 | RESULTS

### 3.1 | Among brain-resident cell types, astrocytes are major IFN-β producers upon in vitro TBEV infection

To investigate the permissiveness of murine CNS-resident cell subsets to TBEV infection, primary neurons, microglia and astrocytes isolated from C57BL/6 (WT) mice were exposed to TBEV Neudoerfl strain in cell culture at MOI 1. After 12 hr of incubation, all three cell types showed TBEV infection, as indicated by replication foci that were detected in perinuclear regions of the cytoplasm of infected cells (Figure 1a, Figure S1). Approximately 40% of the neurons displayed such replication foci, whereas among astrocytes and microglia only 26% and 18% of the cells were infected, respectively (Figure 1b). Quantification of IFN-β protein levels in the SNs revealed that at 12 hr post-infection (hpi) astrocytes produced significantly higher amounts of IFN-β than neurons and microglia (Figure 1c). Thus, upon TBEV exposure, neurons showed a high percentage of infected cells and produced less IFN-β, whereas astrocytes showed lower percentages of infected cells and produced the highest amounts of IFN-β of the analyzed cell types.

### 3.2 | MAVS signaling drives early innate responses in TBEV-infected astrocytes

Transcriptome analyses of TBEV-infected primary astrocytes verified the astrocytic identity of the analyzed cells (Figure S2). At 12 hpi 458 differentially regulated transcripts were identified, of which 439 were up- and 19 downregulated when compared with mock-treated cells (Figure 2a). The upregulated transcripts encoded mostly interferons as well as interferon-stimulated genes, while the downregulated transcripts were none immunoregulatory genes. A gene enrichment analysis of the 458 regulated genes indicated that TBEV-infected astrocytes strongly upregulated genes involved in IFN-signaling pathways, including IFN genes as well as genes involved in the RLR-signaling pathway (Figure 2b). Furthermore, normalized gene counts for *Ddx58*, *Eif2ak2*, and *Ifih1* confirmed the induction of RLR-signaling related genes (Figure 2c–e). Collectively, these data indicated that astrocytes respond to TBEV infection by upregulation of IFN-dependent anti-viral genes, and that RLR signaling presumably is of key relevance for virus sensing and the induction of antiviral responses.

### 3.3 | MAVS signaling is required to restrict TBEV replication in infected astrocytes

To further address the role of RLR signaling, we analyzed murine astrocytes isolated from mice that were deficient of MAVS, the adaptor of RLR signaling. Upon exposure to TBEV strain Neudoerfl at MOI 1, approximately 30% of WT and more than 50% of MAVS ko astrocytes were infected at 12 hpi (Figure 3a), respectively, as indicated by the presence of replication foci (Figure 3b). Quantification of the replication foci by determining their overall mean fluorescence intensity (MFI) revealed that 12 hpi WT astrocytes displayed low dsRNA signals, while MAVS ko astrocytes showed significantly higher signal intensities (Figure 3c). These data indicated that MAVS ko astrocytes showed higher TBEV replication

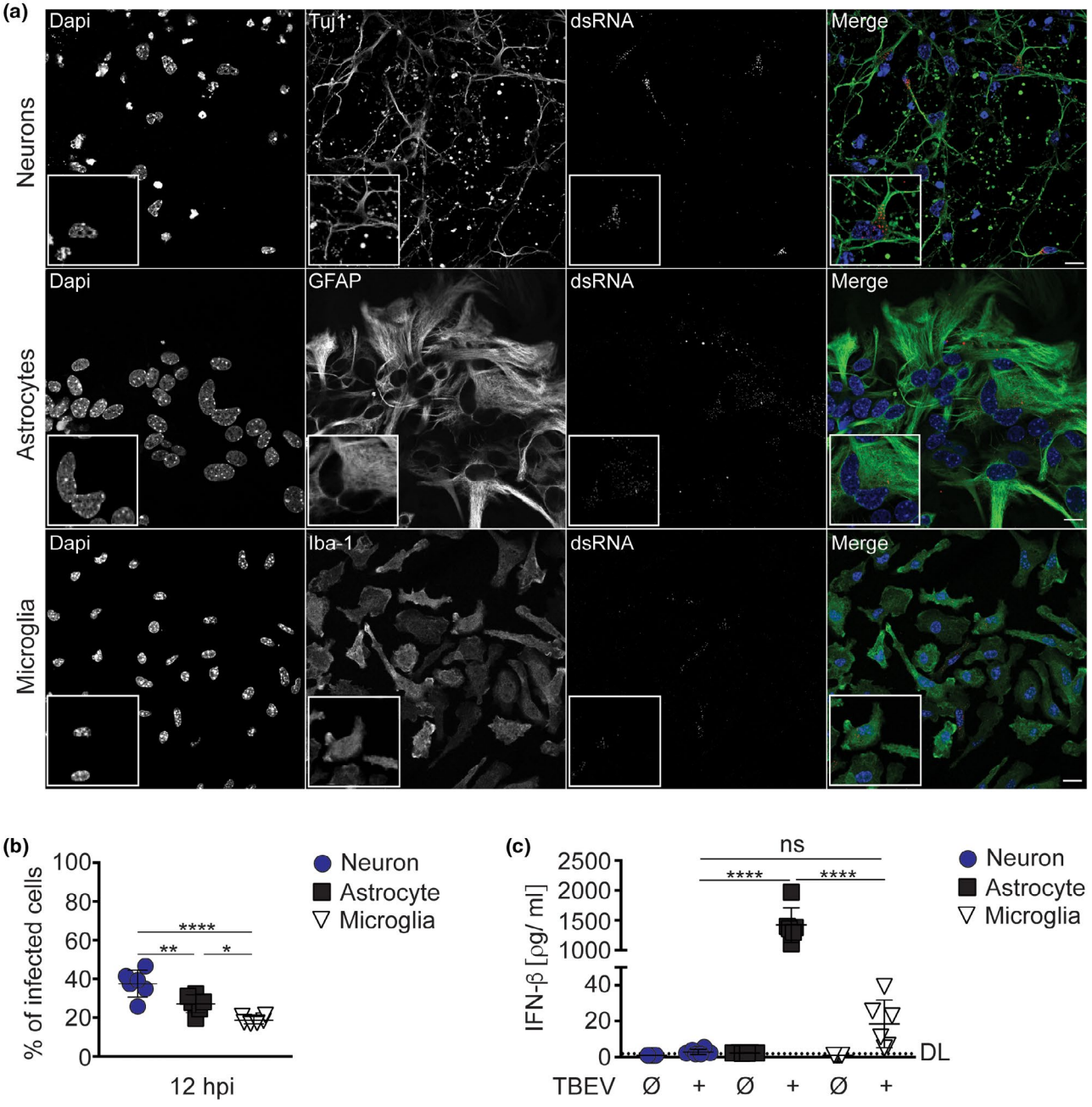


**FIGURE 1** CNS-resident cell types show diverse responses to in vitro TBEV infection. Primary murine neurons, astrocytes, and microglia isolated from C57BL/6 (WT) mice were infected with TBEV Neudoerfl strain at MOI 1. (a) At 12 hpi cells were immunolabeled with either anti-Tuj1 (neurons), anti-GFAP (astrocytes), or anti-Iba1 (microglia) and anti-dsRNA (J2, Scicons English and Scientific Consulting, TBEV replication foci) and counterstained with DAPI. In the lower left corner a blow up of the image is shown (white square). Scale bar 20 μm. (b) Quantification of TBEV-infected neurons, astrocytes, and microglia at 12 hpi displayed as percentage of infected cells ($n = 6$, combined data from three independent experiments). (c) IFN-β protein levels in the SN of cultured primary neurons, astrocytes, and microglia at 12 hr post-TBEV infection was determined by ELISA ($n \geq 5$, combined data from three independent experiments). DL = Detection limit (0.94 pg/ml), error bars indicate mean ± *SD*; ns = not significant; $^{*}p < 0.05$, $^{**}p < 0.01$; $^{***}p < 0.001$; $^{****}p < 0.0001$; One-way ANOVA with Tukey's multiple comparison test; (b), $F(2, 15) = 21.55, p < 0.0001$; (c), $F(2, 15) = 141.5$, $p < 0.0001$

than WT astrocytes. Similarly, 24 hpi WT astrocytes were significantly less infected than MAVS ko astrocytes (Figure 3d), with 50% of WT and 85% of MAVS ko astrocytes being infected, respectively (Figure 3e). Moreover, quantification of TBEV replication foci 24 hpi revealed an overall higher virus replication than at 12 hpi, and MAVS ko astrocytes showed significantly higher numbers of TBEV replication foci than WT astrocytes (Figure 3f). At 12 hpi, similar numbers of TBEV copies were detected in the SN of infected WT and MAVS ko astrocytes, whereas at 24 hpi the number of TBEV copies was significantly enhanced in the SN

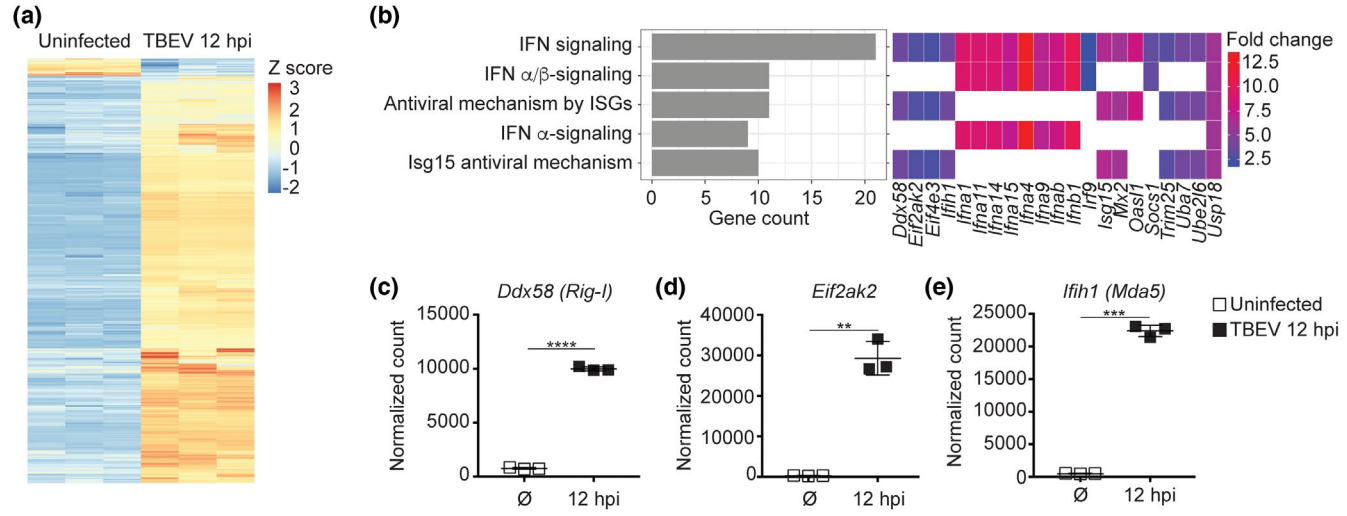


**FIGURE 2** TBEV-infected astrocytes show MAVS-dependent induction of early anti-viral responses. Primary murine astrocytes were either infected with TBEV Neudoerfl strain at MOI 1 or mock treated. At 12 hr post-treatment, RNA-seq analysis was performed. (a) Heatmaps showing relative expression of transcripts obtained from transcriptome analysis of mock-treated (∅) or 12 hr TBEV-infected astrocytes (columns represent biological replicates). (b) Enrichment analysis of significantly expressed genes in TBEV-infected versus mock-treated astrocytes, showing the top 5 enriched reactome pathways. On the *x* axes, the gene counts associated with each pathway are shown. On the right side, the single genes associated with each pathway with the relative fold induction in 12 hr TBEV-infected astrocytes compared to mock treatment. (c–e) Graphs showing normalized reads of genes associated with IFN-related pathways in uninfected and 12 hr TBEV-infected astrocytes (each square represents a biological replicate, $n = 3$; error bars indicate mean ± *SD*; $^{**}p < 0.01$; $^{***}p < 0.001$; $^{****}p < 0.0001$; Two-tailed Unpaired *t* test with Welch's correction)

of MAVS ko astrocytes when compared with the SN of WT astrocytes (Figure 3g). Quantification of TBEV plaque forming units (PFUs) in the SN of infected WT and MAVS ko astrocytes revealed no major differences at 12 hpi and 24 hpi, while at 48 hpi higher virus titers were detected in the SN of MAVS ko astrocytes than in WT astrocytes (Figure 3h). Moreover, infected WT astrocytes produced high amounts of IFN-β already at 12 hpi, which did not further increase until 24 hpi (Figure 3i). In contrast, MAVS ko astrocytes produced very little amounts of IFN-β at 12 hpi, whereas at 24 hpi IFN-β levels increased to moderate levels (Figure 3i). These data supported the hypothesis that in TBEV-infected astrocytes initially MAVS signaling and later other mechanisms drive IFN-β expression.

## 3.4 | Functional MAVS signaling by astrocytes is required for the induction of early IFN and ISG responses

Principal component analysis of transcriptome data of infected and uninfected WT and MAVS ko astrocytes showed that the transcriptomes of uninfected WT and MAVS ko astrocytes clustered closely together, whereas infection led to an increased variance at 12 hpi as well as 24 hpi (Figure 4a). While uninfected controls displayed comparable gene counts independently of whether the analyzed astrocytes were MAVS competent or deficient, 12 and 24 hpi WT astrocytes showed substantially higher gene counts than MAVS ko astrocytes (Figure S3a). TBEV infection induced upregulation of several genes in WT and MAVS ko astrocytes at 12 and 24 hpi (Figure S3b). Comparative analysis of differentially expressed genes (DEGs) at 12 hpi revealed 437 DEGs in WT astrocytes and only 212 DEGs in MAVS ko astrocytes. Two hundred and six transcripts were common between WT and MAVS ko infected astrocytes, while 267 DEGs were only found in infected WT astrocytes (Figure 4b). Similarly, 24 hpi WT and MAVS ko astrocytes displayed 632 and 314 DEGs, respectively, of which 274 were common (Figure 4b). To investigate the impact of MAVS signaling on anti-viral genes, a direct comparison of the transcriptomes of WT and MAVS ko infected astrocytes was performed. At 12 hpi, WT astrocytes showed higher induction of *Ifnb1*, *Ifnab*, *Ifna2-4-5*, and ISGs than MAVS ko astrocytes (Figure 4c). Similarly, at 24 hpi IFN genes and cytokines were found to be more abundantly induced in WT than in MAVS ko astrocytes (Figure 4d). Furthermore, MAVS ko astrocytes showed decreased induction of various cytokines and chemokines at 12 and 24 hpi (Figure S3c). Interestingly, *Il1b* and *Cxcl5* were upregulated only in infected MAVS ko astrocytes, but not in WT astrocytes (Figure S3c). Since lower IFN-β protein levels were detected at 12 and 24 hpi in the SNs of MAVS ko astrocytes than in WT astrocytes, and at 24 hpi MAVS ko astrocytes produced similar amounts of IFN-β as WT astrocytes at 12 hpi (Figure 3i), we next investigated whether MAVS ko astrocytes showed delayed induction of IFN genes. Indeed, 12 hpi MAVS ko astrocytes showed less abundantly induced *Ifnb1*, *Ifna2*, and *Ifna4* genes than WT astrocytes (Figure 4e), whereas the induction of IFN genes was stronger in MAVS ko astrocytes 24 hpi than 12 hpi (Figure 4e). Similarly, at 12 hpi interferon-stimulated genes such as *Isg15*, *Mx1*, and *Rasd2* were less abundantly induced in MAVS ko astrocytes than in WT astrocytes, while at 24 hpi these gene were also induced in MAVS ko astrocytes (Figure 4e). In line

with these observations, the number of TBEV transcripts was significantly higher in MAVS ko astrocytes than in WT astrocytes at 24 hpi (Figure 4f). Together, these data indicate that the lack of MAVS signaling is associated with reduced induction of IFN-β, IFN-αs, and ISGs, which allows enhanced viral replication that further impairs the intrinsic response of astrocytes to TBEV infection.

### 3.5 | IFN-β induction in infected astrocytes is dependent on sequential MAVS and MyD88/TRIF signaling

To further elucidate to what extent MAVS signaling contributes to the induction of innate immune responses, pathways that were

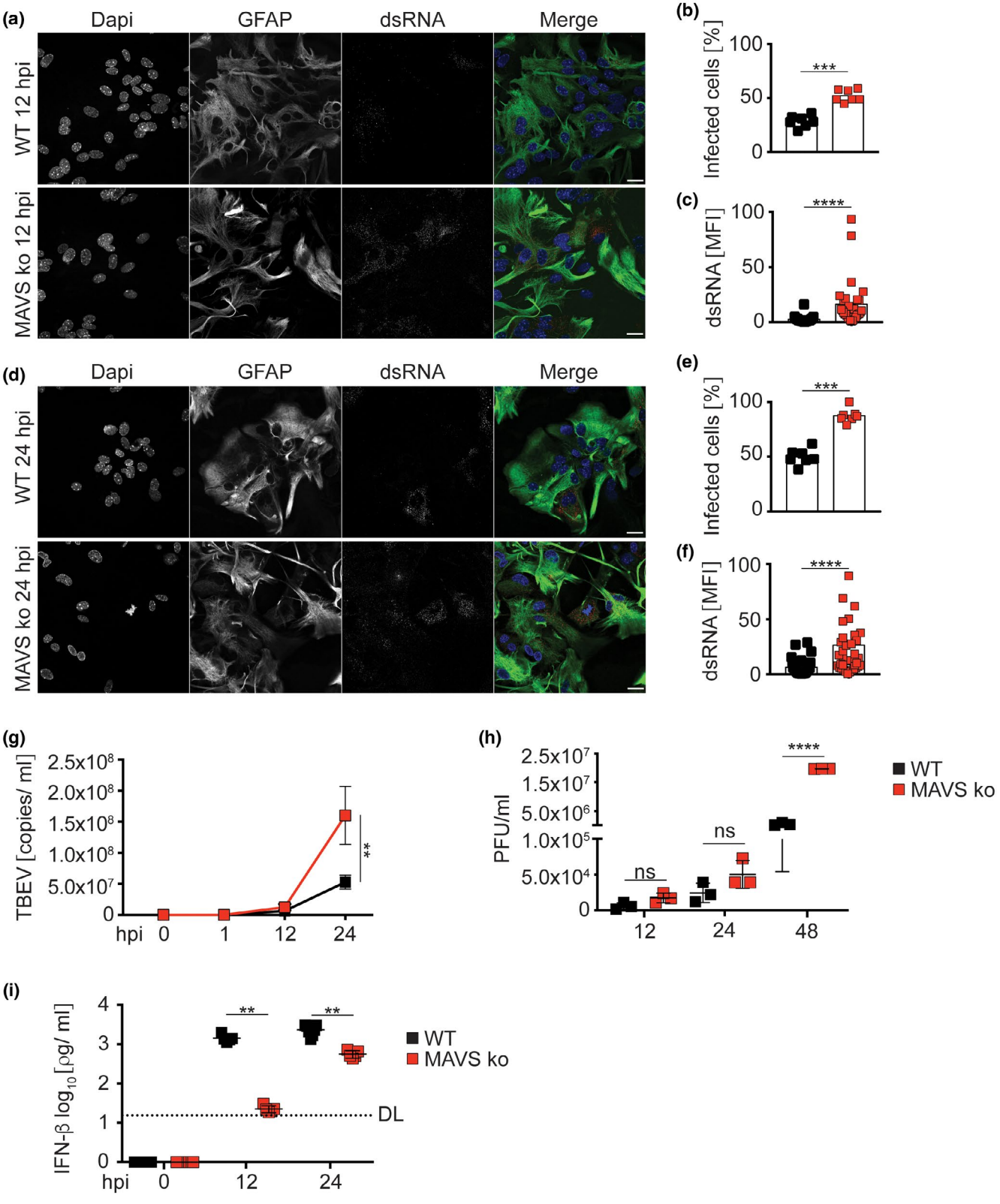

**FIGURE 3** MAVS-deficient astrocytes fail to curtail TBEV replication. Primary murine astrocytes isolated from WT or MAVS ko mice were infected with TBEV Neudoerfl strain at MOI 1. (a, c) At 12 and 24 hpi WT and MAVS ko astrocytes were immunolabeled with anti-GFAP, anti-dsRNA antibodies and counterstained with DAPI and immunofluorescence microscopy was performed, scale bar 20 μm. (b, e) Quantification of WT and MAVS ko TBEV-infected astrocytes at 12 and 24 hpi, graphs displayed percentage of infected cells ($n = 6$, combined data from three independent, bar plot indicates mean + *SD*). (c, f) dsRNA mean fluorescence intensity (MFI) within infected cells as a measure of TBEV replication foci at 12 and 24 hpi ($n = 6$, combined data from three independent experiments, bar plot indicates mean + *SD*). (g) TBEV copies per ml in the SN of WT and MAVS ko astrocytes at 0, 1, 12, and 24 hpi quantified by RT-qPCR ($n \geq 5$, combined data from three independent experiments). (h) Viral titer from SNs of WT and MAVS ko TBEV-infected astrocytes at 12, 24, and 48 hpi shown as plaque forming unit (PFU) per ml ($n = 3$, combined data from two independent experiments). (i) IFN-β protein expression in the SN of WT and MAVS ko astrocytes at 12 and 24 hr post-TBEV infection was determined by ELISA ($n \geq 5$, combined data from three independent experiments) DL = Detection limit (16 pg/ml). Error bars indicate mean ± *SD*; $^{*}p < 0.05$, $^{**}p < 0.01$, $^{***}p < 0.001$, $^{****}p < 0.0001$; (b, c, e, f, g, i) Two-tailed Mann–Whitney test, (h) One-way ANOVA with Tukey's multiple comparison test, $F(5, 12) = 6{,}021$, $p < 0.0001$

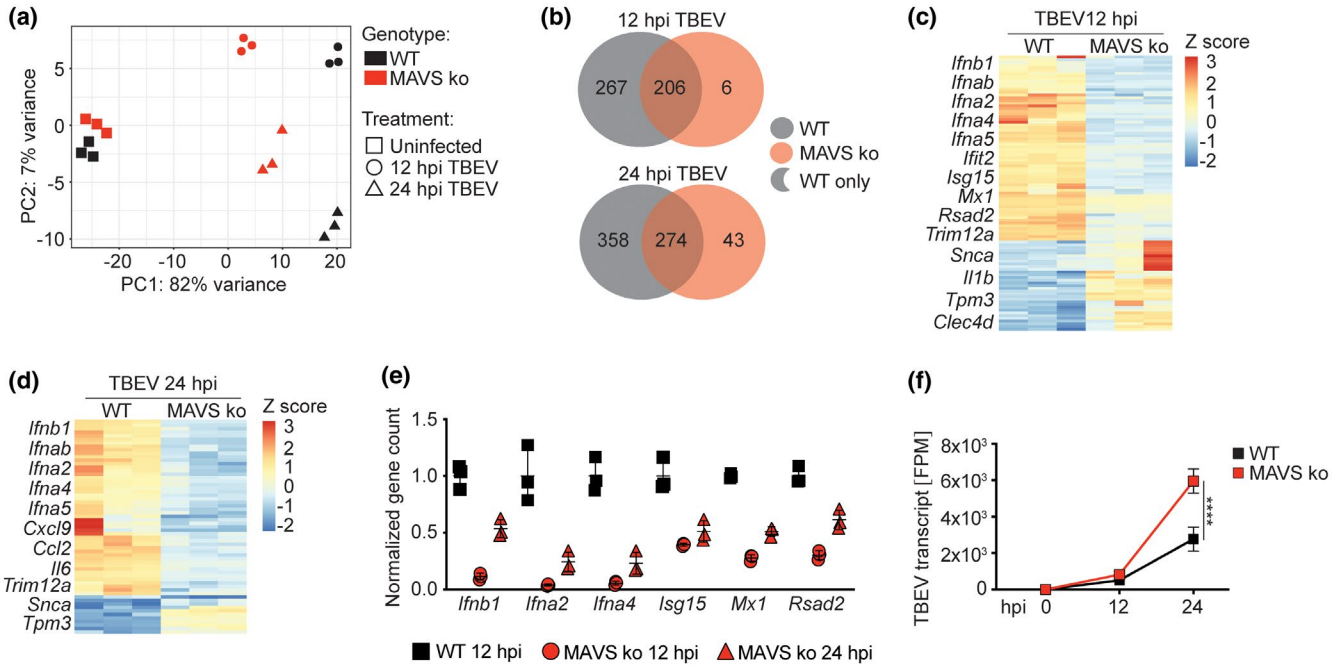


**FIGURE 4** MAVS-deficient astrocytes show impaired anti-viral responses to TBEV infection. Primary murine astrocytes from WT and MAVS ko mice were either mock treated or infected with TBEV Neudoerfl strain at MOI 1. At 12 and 24 hr post-treatment, cells were collected and RNA-seq analysis was performed. (a) Principal component (PC) analysis of WT and MAVS ko astrocytes mock treated or TBEV infected for 12 and 24 hr (each dot represents one individual sample). (b) Venn diagram showing the number of differentially expressed genes (DEGs) between the transcriptomes of WT and MAVS ko astrocytes at 12 and 24 hpi. (c) Heatmap showing relative expression of statistically significant transcripts obtained from transcriptome analysis of WT and MAVS ko astrocytes at 12 hpi (cutoffs: absolute $\log_2$ fold change >2, each column represents transcripts obtained from one individual sample). (d) Heatmap showing relative expression of statistically significant transcripts obtained from transcriptome analysis of WT and MAVS ko astrocytes at 24 hpi (cutoffs: absolute $\log_2$ fold change >2, each column represents transcripts obtained from one individual sample). (e) Dot plots display *Ifnb1*, *Ifna2*, *Ifna4 Isg15*, *Mx1*, and *Rasd2* gene expression in MAVS ko TBEV-infected astrocytes at 12 and 24 hpi in relation to TBEV-infected WT 12 hpi. Gene count values were normalized to TBEV-infected WT 12 hpi with an assigned value of 1 ($n = 3$). (f) Graph depicts transcripts of TBEV in WT and MAVS ko astrocytes at 0, 12 and 24 hpi ($n = 3$ combined data). TPM = transcripts per million. $^{****}p < 0.0001$, ordinary two-way ANOVA with Sidak's multiple comparisons test (interaction $F(3, 40) = 28.52$, $p < 0.0001$)

upregulated upon TBEV infection in WT, but not in MAVS ko astrocytes were investigated. This analysis revealed that at 12 hpi multiple pathways related to innate immunity were dependent on functional MAVS signaling, including cytokine-mediated signaling, immune effector processes, regulation of innate immune responses, and the JAK-STAT cascade (Figure 5a). At 24 hpi, MAVS-dependent signaling pathways were associated with adaptive immunity such as cell–cell adhesion, adaptive immune responses, and lymphocyte differentiation (Figure 5a). Interestingly, 24 hpi pathways related to innate immune responses were not dependent on MAVS signaling, pointing toward the activation of MAVS-independent signaling. To investigate whether MyD88/TRIF signaling contributed to

the induction of protective IFN-β at later stages of in vitro TBEV infection, WT and MAVS astrocytes were treated with MyD88 and TRIF inhibitors, then infected with TBEV and IFN-β protein levels in the SNs were determined by ELISA. SNs of infected WT astrocytes that were not treated with inhibitors contained IFN-β at 12, 24, and 48 hpi (Figure 5b), whereas SNs of infected MAVS ko astrocytes showed significantly lower IFN-β levels at 12 and 24 hpi than WT astrocytes and similar levels as WT astrocytes at 48 hpi (Figure 5b). Upon treatment with MyD88 and TRIF inhibitors, infected WT astrocytes showed reduced IFN-β levels at 12 hpi that were further decreased at 24 hpi and undetectable at 48 hpi (Figure 5c), whereas in the SNs of infected MAVS ko astrocytes no IFN-β was detectable at any of the tested time points (Figure 5c). Since MAVS-independent pathways conferred the induction of late IFN-β, we hypothesized that TLR stimulation via MyD88/TRIF signaling pathways might be relevant. Previous studies showed that astrocytes do not express the single-stranded RNA sensor TLR7 (Trudler et al., 2010). In contrast, *Tlr3* was upregulated upon TBEV infection of astrocytes, whereas this effect was stronger in WT than in MAVS ko astrocytes at 12 hpi (Figure 5d). Furthermore, TRIF (*Ticam1*), the adaptor of *Tlr3*, was moderately upregulated in both infected WT and MAVS ko astrocytes (Figure 5d). Similarly, MyD88 was upregulated in infected WT and MAVS ko astrocytes with a significantly higher induction in WT astrocytes at 12 hpi than in MAVS ko astrocytes (Figure 5d). In conclusion, our data are compatible with the model of a bi-phasic induction of anti-viral responses in TBEV-infected astrocytes, while at early time points MAVS signaling and at later time points MyD88/TRIF signaling is critically needed.

## 4 | DISCUSSION

Astrocytes are major IFN-β producers during CNS infection with a whole variety of RNA-encoded viruses, including WNV (Lindqvist et al., 2016), vesicular stomatitis virus (VSV (Detje et al., 2015)), and rabies virus (RABV (Pfefferkorn et al., 2016)). Here, we observed that upon in vitro TBEV infection of murine brain-derived cell subsets, neurons showed the highest extent of infection and little IFN-β production. In contrast, astrocytes and microglia were less permissive to TBEV infection and produced significantly higher levels of IFN-β. Since astrocytes turned out to be the major IFN-β producers after TBEV infection, we further investigated the underlying mechanisms.

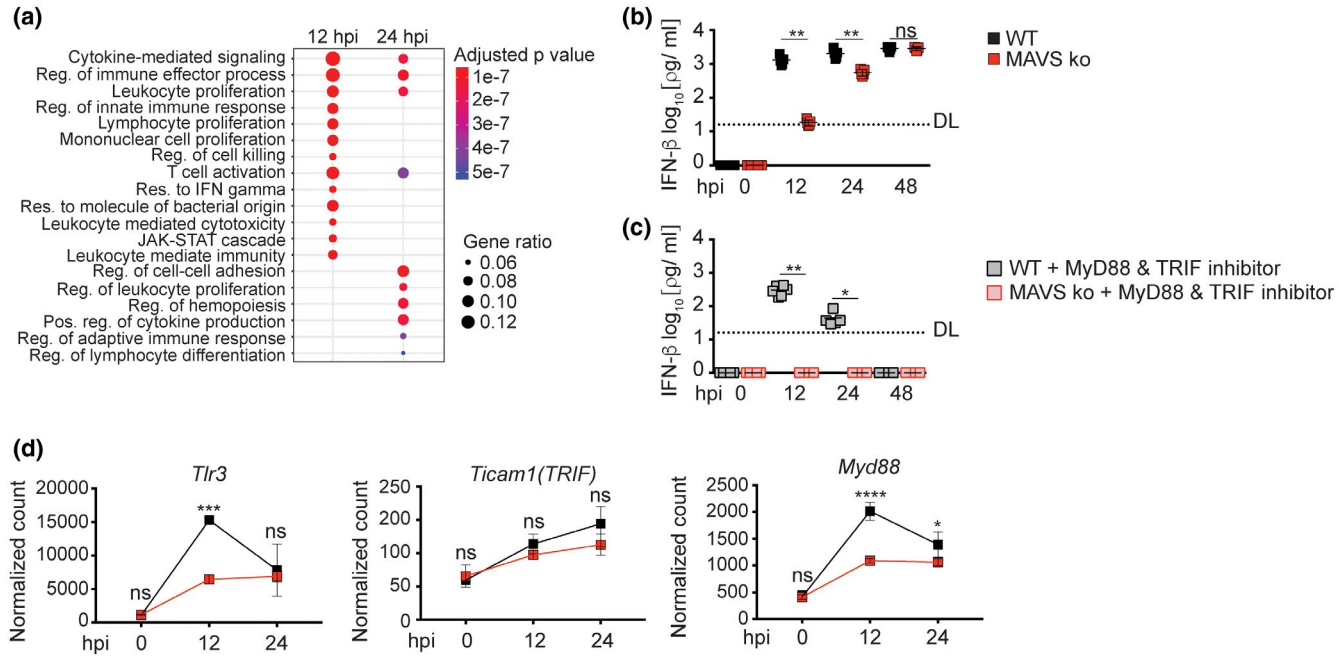


**FIGURE 5** TBEV-induced IFN-β responses of astrocytes initially depend on MAVS and later on MyD88/TRIF signaling. (a) Pathway analysis showing top 20 downregulated GO terms imported from a gene set enrichment analysis (GSEA) of infected MAVS ko astrocytes compared with WT astrocytes at 12 and 24 hpi. The dot size indicates gene ratio, the number of genes within this GO term in comparison to the total number of upregulated genes. (b) WT and MAVS ko astrocytes were infected with TBEV and IFN-β protein level were determined by ELISA at 0, 12, 24, and 48 hpi. (c) WT and MAVS ko astrocytes were pre-treated with MyD88 and TRIF inhibitors (5 μM) for 8 hr, then infected with MOI 1 of TBEV. At 0, 12, 24, and 48 hpi IFN-β protein level were determined by ELISA (untreated sample are the same as depicted in Figure 3h, for (b, c) $n \geq 4$, combined data; DL = Detection limit (16 pg/ml); error bars indicate mean ± *SD*; ns = not significant, $^{*}p < 0.05$, $^{**}p < 0.01$; two-tailed Mann–Whitney test). (d) Graphs showing *Tlr3*, *Ticam1*, *and Myd88* normalized gene counts in uninfected and 12 and 24 hr TBEV-infected WT and MAVS ko astrocytes (each square represents mean value of three biological replicates; error bars indicate mean ± *SD*; ns = not significant; $^{*}p < 0.05$; $^{**}p < 0.01$; $^{***}p < 0.001$; $^{****}p < 0.0001$; ordinary two-way ANOVA with Sidak's multiple comparisons test; *Tlr3* interaction $F(2, 12) = 13.13$, $p = 0.0010$; *Ticam1* interaction $F(2, 12) = 1.318$, $p = 0.3038$; *Myd88* interaction $F(2, 12) = 21.27$, $p = 0.0001$)

Transcriptome analyses revealed that early after infection signaling of MAVS, the adaptor of RLRs, is needed to induce IFNs and anti-viral responses in astrocytes. Consistently, astrocytes isolated from MAVS-deficient mice showed increased TBEV replication as well as substantially decreased IFN-β induction early after infection. Interestingly, at later time points MAVS-independent and MyD88/TRIF-dependent mechanisms triggered almost normal anti-viral responses. These data support the hypothesis that TBEV-infected murine astrocytes mount anti-viral responses in a bi-phasic manner that initially is driven by MAVS and later by MyD88/TRIF signaling.

In case of flavivirus infection, in vivo as well as in vitro experiments indicated that IFN responses are important to limit virus replication and to support recovery from the infection (Best et al., 2005; Diamond et al., 2000; Lin et al., 2004; Robertson et al., 2009). Accordingly, TBEV-infected murine astrocytes mount rapid IFN responses (Lindqvist et al., 2016, 2018), whereas IFNAR-deficient murine astrocytes showed increased virus replication and cytopathic effects (Lindqvist et al., 2016). As a consequence of the induction of IFN responses and activation of JAK-STAT signaling, ISGs are induced (Ihle, 1995; Platanias, 2005). Among ISGs that confer anti-viral effects during flavivirus infection, *Oas1* was shown to cleave viral mRNA (Perelygin et al., 2002). Similarly, viperin was reported to be induced in astrocytes, and to be involved in proteasome-dependent degradation of TBEV and Zika virus (ZIKV) NS3, thus restricting TBEV replication and spread (Lindqvist et al., 2018; Panayiotou et al., 2018; Upadhyay et al., 2017). We found that TBEV showed sustained replication in MAVS ko astrocytes and that substantially reduced RNA levels of IFNs and ISGs, including *Oas1* and *Rsad2* (viperin), were induced. TRIM5a has previously been shown to contribute to the restriction of infection with TBEV and other flaviviruses in murine astrocytes (Chiramel et al., 2019). Interestingly, in our experiments *Trim12a*, which is the truncated murine homolog of human TRIM5a (Chang et al., 2015), was induced in TBEV-infected WT astrocytes at early and late time points, whereas its induction was not detectable in MAVS ko astrocytes.

Earlier studies already suggested a key role of MAVS during LGTV infection, as indicated by MAVS ko mice that succumbed to systemic infection and showed higher viral loads and accelerated virus spread within the CNS (Kurhade et al., 2016). However, in these experiments, cytokine levels in brain homogenates of LGTV-infected MAVS ko mice were similar as in WT animals at 4 dpi (Kurhade et al., 2016), suggesting that by that time MAVS-independent mechanisms must have been in place to trigger cytokine induction within the CNS. Upon RNA virus infection, the viral RNA is recognized by TLRs or RLRs including RIG-I and MDA5 (Loo & Gale, 2011). RLR signaling has previously been shown to play a key role in initiating immune responses upon flavivirus infection such as WNV, DENV, and others (Fredericksen et al., 2008; Nasirudeen et al., 2011; Perry et al., 2009). Indeed, in case of in vitro WNV infection, RIG-I and MDA5 were shown to be engaged by viral PAMPs that arose during virus replication (Fredericksen & Gale, 2006; Shipley et al., 2012). In line with these studies, we showed here that in astrocytes induction of early anti-viral responses relies on MAVS signaling, whereas at later stages of infection also MyD88/TRIF signaling was important. Among TLRs, TLR3 and TLR7 have previously been shown to be involved in flavivirus sensing, which for downstream signaling deploy the adaptors TRIF and MyD88, respectively (Suthar et al., 2013). However, from these TLRs astrocytes only express TLR3 (Trudler et al., 2010). Whereas TLR3 signals via the adaptor molecule TRIF (Yamamoto et al., 2003), MyD88 is the adaptor of all other TLRs and of the IL-1 receptor family (Adachi et al., 1998; Kawai & Akira, 2010). While it is still unclear which viral PAMPs trigger TLR3 during flavivirus infection, previous studies showed that in the case of WNV and DENV, TLR3 is involved in the induction of anti-viral responses (Nasirudeen et al., 2011; Suthar et al., 2013; Tsai et al., 2009). Also, the inflammasome has been shown to contribute to the induction of anti-viral responses during WNV and DENV infection (Guerrero et al., 2013; Ramos et al., 2012; Wu et al., 2013). However, the signal triggering IL-1β expression still has not been uncovered, yet. Here we found that MAVS ko astrocytes show reduced and delayed responses to TBEV infection. Nonetheless, TBEV-infected MAVS ko astrocytes upregulate *Tlr3*, *Ticam1*, and *Myd88* genes as well as the gene encoding for IL-1β thus highlighting a possible explanation for the involvement of MyD88/TRIF signaling during the induction of late anti-viral responses. Further studies are needed to reveal whether late anti-viral responses of MAVS ko astrocytes involve the TLR3-TRIF and/or the IL-1β-MyD88 axis.

Similar to the mouse system, within TBEV-infected human neurons, the virus replicates, spreads, and induces cytopathic effects (Bílý et al., 2015; Růžek et al., 2011). Human astrocytes show sustained TBEV infection and virus replication without the induction of cytopathic effects or cell death until 14 dpi (Palus et al., 2014; Potokar et al., 2014). Recently it was shown that human neurons and astrocytes differentially respond to TBEV infection. While neurons were more susceptible to the infection and showed reduced immune responsiveness, astrocytes were more resistant to the infection and mounted stronger anti-viral responses. Moreover, astrocytes contributed to neuronal protection against TBEV infection (Fares et al., 2020; Pokorna Formanova et al., 2019). During TBEV infection of human astrocytes, the RLRs RIG-I and MDA5, but not TLR3, sense TBEV NS5 and activate IRF-3 signaling, which leads to the production of CCL5 (Zheng et al., 2018). A recent study analyzing RNA expression profiles of TBEV-infected human neuro-glia cultures, that is, neuron and astrocyte cocultures, showed that in astrocytes the transcripts of *Ddx58*, *Oas2*, *IFN-β*, *Mx1*, *Trim5a*, and *Rasd2* were even more abundantly induced than in neurons (Fares et al., 2020). We also observed upregulation of these transcripts in TBEV-infected WT astrocytes, whereas in MAVS ko astrocytes the induction of the respective transcripts was significantly decreased.

Fares et al. showed that at early stages of the infection, human TBEV-infected astrocytes show TLR3 expression that is close to basal levels, whereas at 24 hpi TLR3 expression is significantly enhanced (Fares et al., 2020). We also observed induction of TLR3 upon infection of both, WT and MAVS ko astrocytes. Interestingly, a previous study showed that in humans a functional TLR3 is a risk factor for the development of encephalitis during TBEV infection

(Kindberg et al., 2011). In contrast, mouse studies with other flaviviruses such as WNV and ZIKV revealed a protective role of TLR signaling (Sabouri et al., 2014; Vanwalscappel et al., 2018), highlighting the need of additional studies to define the role of TLR signaling during TBEV infection.

The sequential role of MAVS and TLR signaling in inducing early anti-viral immunity as described here, is in accordance with a study form Hotz et al., where a reprogramming mechanism of TLR and RLR signaling upon viral infection was described (Hotz et al., 2015). Indeed, the authors found that upon Sendai virus infection of murine APCs, RLR-mediated IFN responses were abolished within 24 hr but an increased TLR-dependent response was observed suggesting the presence of reprogramming mechanism in favor of TLR over RLR signaling (Hotz et al., 2015). Thus, it is possible that also TLR and RLR signaling of astroicytes undergo a reprogramming mechanism during the anti-viral response to TBEV infection, nevertheless further studies are needed to clarify this phenomena.

Taken together, upon in vitro TBEV infection of mouse-derived brain-resident cell subsets, astrocytes are the main IFN-β producers. Early after infection, astrocytes are stimulated in a MAVS-dependent manner, presumably via RLR signaling, whereas at later time points MyD88/TRIF signaling was needed. These observations indicate that sensing of single pathogens involves multiple mechanisms not only in different tissues during the course of an infection (Spanier et al., 2014; Tegtmeyer et al., 2019), but that even in one and the same cell subset distinct sensing mechanisms can be relevant at different times after infection.

## DECLARATION OF TRANSPARENCY

The authors, reviewers and editors affirm that in accordance to the policies set by the *Journal of Neuroscience Research*, this manuscript presents an accurate and transparent account of the study being reported and that all critical details describing the methods and results are present.

### ACKNOWLEDGMENTS

We thank Jennifer Skerra and Kira Baumann for help with mouse breeding and screening. We thank Carla Schmutte for excellent technical support.

### ETHICS APPROVAL AND CONSENT TO PARTICIPATE

All mice were bred and kept under specific pathogen-free conditions in the central mouse facility of the Helmholtz Centre for Infection Research, Brunswick, and at TWINCORE, Centre for Experimental and Clinical Infection Research, Hanover, Germany. Mouse experimental work was carried out in compliance with regulations of the German Animal Welfare Law.

### CONFLICT OF INTEREST

The authors declare no conflict of interest.

### AUTHOR CONTRIBUTIONS

*Conceptualization*, L.G., I.S. and U.K.; *Methodology*, L.G., V.B., A.P., F.M., O.G., C.K.P., I.S., and U.K.; *Investigation*, L.G., V.B., A.P., F.M., O.G., I.S.; *Data Curation*, L.G., V.B., F.M., A.P., O.G., V.D., M.K., K.J., M.S., I.S. and U.K.; *Writing – Original Draft*, L.G., I.S. and U.K., *Supervision*, I.S. and U.K.; *Funding Acquisition*, K.J., M.S., I.S. and U.K.

### PEER REVIEW

The peer review history for this article is available at https://publons.com/publon/10.1002/jnr.24923.

### DATA AVAILABILITY STATEMENT

The gene expression profiling data that support the findings of this study are available in NCBI's Gene Expression Omnibus (RRID:SCR_005012) and are accessible through GEO Series accession number GSE175823. Further data supporting the findings of this study are available from the corresponding author upon reasonable request.

### ORCID

*Luca Ghita* https://orcid.org/0000-0001-6736-6355
*Ulrich Kalinke* https://orcid.org/0000-0003-0503-9564

### REFERENCES

Adachi, O., Kawai, T., Takeda, K., Matsumoto, M., Tsutsui, H., Sakagami, M., Nakanishi, K., & Akira, S. (1998). Targeted disruption of the MyD88 gene results in loss of IL-1- and IL-18-mediated function. *Immunity*, *9*, 143–150. https://doi.org/10.1016/S1074-7613(00)80596-8

Beaute, J., Spiteri, G., Warns-Petit, E., & Zeller, H. (2018). Tick-borne encephalitis in Europe, 2012 to 2016. *Euro Surveillance: Bulletin Europeen sur les Maladies Transmissibles = European Communicable Disease Bulletin*, *23*, 1800201.

Beissbarth, T., & Speed, T. P. (2004). GOstat: Find statistically overrepresented gene ontologies within a group of genes. *Bioinformatics*, *20*, 1464–1465. https://doi.org/10.1093/bioinformatics/bth088

Best, S. M., Morris, K. L., Shannon, J. G., Robertson, S. J., Mitzel, D. N., Park, G. S., Boer, E., Wolfinbarger, J. B., & Bloom, M. E. (2005). Inhibition of interferon-stimulated JAK-STAT signaling by a tick-borne flavivirus and identification of NS5 as an interferon antagonist. *Journal of Virology*, *79*, 12828–12839. https://doi.org/10.1128/JVI.79.20.12828-12839.2005

Bílý, T., Palus, M., Eyer, L., Elsterová, J., Vancová, M., & Růžek, D. (2015). Electron tomography analysis of tick-borne encephalitis virus infection in human neurons. *Scientific Reports*, *5*, 10745. https://doi.org/10.1038/srep10745

Carty, M., Reinert, L., Paludan, S. R., & Bowie, A. G. (2014). Innate antiviral signalling in the central nervous system. *Trends in Immunology*, *35*, 79–87. https://doi.org/10.1016/j.it.2013.10.012

Chang, T. H., Yoshimi, R., & Ozato, K. (2015). Tripartite motif (TRIM) 12c, a mouse homolog of TRIM5, is a ubiquitin ligase that stimulates type I IFN and NF-κB pathways along with TNFR-associated factor 6. *Journal of Immunology*, *195*, 5367–5379.

Chiramel, A. I., Meyerson, N. R., McNally, K. L., Broeckel, R. M., Montoya, V. R., Méndez-Solís, O., Robertson, S. J., Sturdevant, G. L., Lubick, K. J., Nair, V., Youseff, B. H., Ireland, R. M., Bosio, C. M., Kim, K., Luban, J., Hirsch, V. M., Taylor, R. T., Bouamr, F., Sawyer, S. L., & Best, S. M. (2019). TRIM5α restricts flavivirus replication by targeting the viral protease for proteasomal degradation. *Cell Reports*, *27*, 3269–3283.e6. https://doi.org/10.1016/j.celrep.2019.05.040

Detje, C. N., Lienenklaus, S., Chhatbar, C., Spanier, J., Prajeeth, C. K., Soldner, C., Tovey, M. G., Schlüter, D., Weiss, S., Stangel, M., & Kalinke, U. (2015). Upon intranasal vesicular stomatitis virus infection, astrocytes in the olfactory bulb are important interferon Beta producers that protect from lethal encephalitis. *Journal of Virology*, *89*, 2731–2738. https://doi.org/10.1128/JVI.02044-14

Diamond, M. S., Roberts, T. G., Edgil, D., Lu, B., Ernst, J., & Harris, E. (2000). Modulation of Dengue virus infection in human cells by alpha, beta, and gamma interferons. *Journal of Virology*, *74*, 4957–4966. https://doi.org/10.1128/JVI.74.11.4957-4966.2000

Dobin, A., Davis, C. A., Schlesinger, F., Drenkow, J., Zaleski, C., Jha, S., Batut, P., Chaisson, M., & Gingeras, T. R. (2013). STAR: Ultrafast universal RNA-seq aligner. *Bioinformatics*, *29*, 15–21. https://doi.org/10.1093/bioinformatics/bts635

Dumpis, U., Crook, D., & Oksi, J. (1999). Tick-borne encephalitis. *Clinical Infectious Diseases*, *28*(4), 882–890. https://doi.org/10.1086/515195

Fares, M., Cochet-Bernoin, M., Gonzalez, G., Montero-Menei, C. N., Blanchet, O., Benchoua, A., Boissart, C., Lecollinet, S., Richardson, J., Haddad, N., & Coulpier, M. (2020). Pathological modeling of TBEV infection reveals differential innate immune responses in human neurons and astrocytes that correlate with their susceptibility to infection. *Journal of Neuroinflammation*, *17*, 76. https://doi.org/10.1186/s12974-020-01756-x

Fredericksen, B. L., & Gale, M., Jr. (2006). West Nile virus evades activation of interferon regulatory factor 3 through RIG-I-dependent and -independent pathways without antagonizing host defense signaling. *Journal of Virology*, *80*, 2913–2923. https://doi.org/10.1128/JVI.80.6.2913-2923.2006

Fredericksen, B. L., Keller, B. C., Fornek, J., Katze, M. G., & Gale, M., Jr. (2008). Establishment and maintenance of the innate antiviral response to West Nile Virus involves both RIG-I and MDA5 signaling through IPS-1. *Journal of Virology*, *82*, 609–616. https://doi.org/10.1128/JVI.01305-07

Furr, S. R., Chauhan, V. S., Sterka, D., Jr., Grdzelishvili, V., & Marriott, I. (2008). Characterization of retinoic acid-inducible gene-I expression in primary murine glia following exposure to vesicular stomatitis virus. *Journal of Neurovirology*, *14*, 503–513. https://doi.org/10.1080/13550280802337217

Goubau, D., Deddouche, S., & Reis e Sousa, C. (2013). Cytosolic sensing of viruses. *Immunity*, *38*, 855–869. https://doi.org/10.1016/j.immuni.2013.05.007

Gritsun, T. S., Lashkevich, V. A., & Gould, E. A. (2003). Tick-borne encephalitis. *Antiviral Research*, *57*, 129–146. https://doi.org/10.1016/S0166-3542(02)00206-1

Guerrero, C. D., Arrieta, A. F., Ramirez, N. D., Rodríguez, L. S., Vega, R., Bosch, I., Rodríguez, J. A., Narváez, C. F., & Salgado, D. M. (2013). High plasma levels of soluble ST2 but not its ligand IL-33 is associated with severe forms of pediatric dengue. *Cytokine*, *61*, 766–771. https://doi.org/10.1016/j.cyto.2012.12.024

Heinz, F. X., & Kunz, C. (2004). Tick-borne encephalitis and the impact of vaccination. *Archives of Virology Supplementum* (*18*), 201–205.

Hellenbrand, W., Kreusch, T., Böhmer, M. M., Wagner-Wiening, C., Dobler, G., Wichmann, O., & Altmann, D. (2019). Epidemiology of tick-borne encephalitis (TBE) in Germany, 2001–2018. *Pathogens*, *8*(2), 42.

Hotz, C., Roetzer, L. C., Huber, T., Sailer, A., Oberson, A., Treinies, M., Heidegger, S., Herbst, T., Endres, S., & Bourquin, C. (2015). TLR and RLR signaling are reprogrammed in opposite directions after detection of viral infection. *Journal of Immunology*, *195*(9), 4387–4395.

Hou, F., Sun, L., Zheng, H., Skaug, B., Jiang, Q. X., & Chen, Z. J. (2011). MAVS forms functional prion-like aggregates to activate and propagate antiviral innate immune response. *Cell*, *146*, 448–461. https://doi.org/10.1016/j.cell.2011.06.041

Ihle, J. N. (1995). The Janus protein tyrosine kinase family and its role in cytokine signaling. *Advances in Immunology*, *60*, 1–35.

Kawai, T., & Akira, S. (2010). The role of pattern-recognition receptors in innate immunity: Update on Toll-like receptors. *Nature Immunology*, *11*, 373–384. https://doi.org/10.1038/ni.1863

Kawai, T., & Akira, S. (2011). Toll-like receptors and their crosstalk with other innate receptors in infection and immunity. *Immunity*, *34*, 637–650. https://doi.org/10.1016/j.immuni.2011.05.006

Kerbo, N., Donchenko, I., Kutsar, K., & Vasilenko, V. (2005). Tickborne encephalitis outbreak in Estonia linked to raw goat milk, May-June 2005. *Euro Surveillance: Bulletin Europeen sur les Maladies Transmissibles = European Communicable Disease Bulletin*, *10*, E050623.2.

Kindberg, E., Vene, S., Mickiene, A., Lundkvist, Å., Lindquist, L., & Svensson, L. (2011). A functional Toll-like receptor 3 gene (TLR3) may be a risk factor for tick-borne encephalitis virus (TBEV) infection. *Journal of Infectious Diseases*, *203*, 523–528. https://doi.org/10.1093/infdis/jiq082

Koyuncu, O. O., Hogue, I. B., & Enquist, L. W. (2013). Virus infections in the nervous system. *Cell Host & Microbe*, *13*, 379–393. https://doi.org/10.1016/j.chom.2013.03.010

Kuno, G., Chang, G. J., Tsuchiya, K. R., Karabatsos, N., & Cropp, C. B. (1998). Phylogeny of the genus flavivirus. *Journal of Virology*, *72*, 73–83.

Kurhade, C., Zegenhagen, L., Weber, E., Nair, S., Michaelsen-Preusse, K., Spanier, J., Gekara, N. O., Kroger, A., & Overby, A. K. (2016). Type I Interferon response in olfactory bulb, the site of tick-borne flavivirus accumulation, is primarily regulated by IPS-1. *Journal of Neuroinflammation*, *13*, 22. https://doi.org/10.1186/s12974-016-0487-9

Lani, R., Moghaddam, E., Haghani, A., Chang, L. Y., AbuBakar, S., & Zandi, K. (2014). Tick-borne viruses: A review from the perspective of therapeutic approaches. *Ticks and tick-borne Diseases*, *5*, 457–465. https://doi.org/10.1016/j.ttbdis.2014.04.001

Lin, R. J., Liao, C. L., Lin, E., & Lin, Y. L. (2004). Blocking of the alpha interferon-induced Jak-Stat signaling pathway by Japanese encephalitis virus infection. *Journal of Virology*, *78*, 9285–9294. https://doi.org/10.1128/JVI.78.17.9285-9294.2004

Lindquist, L., & Vapalahti, O. (2008). Tick-borne encephalitis. *Lancet*, *371*, 1861–1871. https://doi.org/10.1016/S0140-6736(08)60800-4

Lindqvist, R., Kurhade, C., Gilthorpe, J. D., & Överby, A. K. (2018). Cell-type- and region-specific restriction of neurotropic flavivirus infection by viperin. *Journal of Neuroinflammation*, *15*, 80. https://doi.org/10.1186/s12974-018-1119-3

Lindqvist, R., Mundt, F., Gilthorpe, J. D., Wolfel, S., Gekara, N. O., Kroger, A., & Overby, A. K. (2016). Fast type I interferon response protects astrocytes from flavivirus infection and virus-induced cytopathic effects. *Journal of Neuroinflammation*, *13*, 277. https://doi.org/10.1186/s12974-016-0748-7

Loo, Y. M., & Gale, M., Jr. (2011). Immune signaling by RIG-I-like receptors. *Immunity*, *34*, 680–692. https://doi.org/10.1016/j.immuni.2011.05.003

Love, M. I., Huber, W., & Anders, S. (2014). Moderated estimation of fold change and dispersion for RNA-seq data with DESeq2. *Genome Biology*, *15*, 550. https://doi.org/10.1186/s13059-014-0550-8

Mandl, C. W., Heinz, F. X., Stöckl, E., & Kunz, C. (1989). Genome sequence of tick-borne encephalitis virus (Western subtype) and comparative analysis of nonstructural proteins with other flaviviruses. *Virology*, *173*, 291–301. https://doi.org/10.1016/0042-6822(89)90246-8

Mansfield, K. L., Johnson, N., Phipps, L. P., Stephenson, J. R., Fooks, A. R., & Solomon, T. (2009). Tick-borne encephalitis virus—A review of an emerging zoonosis. *Journal of General Virology*, *90*, 1781–1794. https://doi.org/10.1099/vir.0.011437-0

McCarthy, G. M., Bridges, C. R., Blednov, Y. A., & Harris, R. A. (2017). CNS cell-type localization and LPS response of TLR signaling pathways. *F1000Research*, *6*, 1144. https://doi.org/10.12688/f1000research.12036.1

Michallet, M.-C., Meylan, E., Ermolaeva, M. A., Vazquez, J., Rebsamen, M., Curran, J., Poeck, H., Bscheider, M., Hartmann, G., König, M., Kalinke, U., Pasparakis, M., & Tschopp, J. (2008). TRADD protein is an essential component of the RIG-like helicase antiviral pathway. *Immunity*, *28*, 651–661. https://doi.org/10.1016/j.immuni.2008.03.013

Nasirudeen, A. M., Wong, H. H., Thien, P., Xu, S., Lam, K. P., & Liu, D. X. (2011). RIG-I, MDA5 and TLR3 synergistically play an important role in restriction of dengue virus infection. *PLoS Neglected Tropical Diseases*, *5*, e926. https://doi.org/10.1371/journal.pntd.0000926

Palus, M., Bílý, T., Elsterová, J., Langhansová, H., Salát, J., Vancová, M., & Růžek, D. (2014). Infection and injury of human astrocytes by tick-borne encephalitis virus. *Journal of General Virology*, *95*, 2411–2426. https://doi.org/10.1099/vir.0.068411-0

Palus, M., Vancova, M., Sirmarova, J., Elsterova, J., Perner, J., & Ruzek, D. (2017). Tick-borne encephalitis virus infects human brain microvascular endothelial cells without compromising blood-brain barrier integrity. *Virology*, *507*, 110–122. https://doi.org/10.1016/j.virol.2017.04.012

Panayiotou, C., Lindqvist, R., Kurhade, C., Vonderstein, K., Pasto, J., Edlund, K., Upadhyay, A. S., & Överby, A. K. (2018). Viperin restricts Zika virus and tick-borne encephalitis virus replication by targeting NS3 for proteasomal degradation. *Journal of Virology*, *92*(7), e02054–17. https://doi.org/10.1128/JVI.02054-17

Perelygin, A. A., Scherbik, S. V., Zhulin, I. B., Stockman, B. M., Li, Y., & Brinton, M. A. (2002). Positional cloning of the murine flavivirus resistance gene. *Proceedings of the National Academy of Sciences of the United States of America*, *99*, 9322–9327. https://doi.org/10.1073/pnas.142287799

Perry, S. T., Prestwood, T. R., Lada, S. M., Benedict, C. A., & Shresta, S. (2009). Cardif-mediated signaling controls the initial innate response to dengue virus in vivo. *Journal of Virology*, *83*, 8276–8281. https://doi.org/10.1128/JVI.00365-09

Pfefferkorn, C., Kallfass, C., Lienenklaus, S., Spanier, J., Kalinke, U., Rieder, M., Conzelmann, K. K., Michiels, T., & Staeheli, P. (2016). Abortively infected astrocytes appear to represent the main source of interferon beta in the virus-infected brain. *Journal of Virology*, *90*, 2031–2038. https://doi.org/10.1128/JVI.02979-15

Platanias, L. C. (2005). Mechanisms of type-I- and type-II-interferon-mediated signalling. *Nature Reviews Immunology*, *5*, 375–386. https://doi.org/10.1038/nri1604

Pokorna Formanova, P., Palus, M., Salat, J., Hönig, V., Stefanik, M., Svoboda, P., & Ruzek, D. (2019). Changes in cytokine and chemokine profiles in mouse serum and brain, and in human neural cells, upon tick-borne encephalitis virus infection. *Journal of Neuroinflammation*, *16*, 205. https://doi.org/10.1186/s12974-019-1596-z

Potokar, M., Korva, M., Jorgačevski, J., Avšič-Županc, T., & Zorec, R. (2014). Tick-borne encephalitis virus infects rat astrocytes but does not affect their viability. *PLoS ONE*, *9*, e86219. https://doi.org/10.1371/journal.pone.0086219

Prajeeth, C. K., Dittrich-Breiholz, O., Talbot, S. R., Robert, P. A., Huehn, J., & Stangel, M. (2018). IFN-gamma producing Th1 cells induce different transcriptional profiles in microglia and astrocytes. *Frontiers in Cellular Neuroscience*, *12*, 352.

Ramos, H. J., Lanteri, M. C., Blahnik, G., Negash, A., Suthar, M. S., Brassil, M. M., Sodhi, K., Treuting, P. M., Busch, M. P., Norris, P. J., & Gale, M. (2012). IL-1β signaling promotes CNS-intrinsic immune control of West Nile virus infection. *PLoS Path*, *8*, e1003039. https://doi.org/10.1371/journal.ppat.1003039

Reed, L. J., & Muench, H. (1938). A simple method of estimating fifty per cent endpoints12. *American Journal of Epidemiology*, *27*, 493–497. https://doi.org/10.1093/oxfordjournals.aje.a118408

Robertson, S. J., Mitzel, D. N., Taylor, R. T., Best, S. M., & Bloom, M. E. (2009). Tick-borne flaviviruses: Dissecting host immune responses and virus countermeasures. *Immunologic Research*, *43*, 172–186. https://doi.org/10.1007/s12026-008-8065-6

Růžek, D., Salát, J., Singh, S. K., & Kopecký, J. (2011). Breakdown of the blood-brain barrier during tick-borne encephalitis in mice is not dependent on CD8+ T-cells. *PLoS ONE*, *6*, e20472. https://doi.org/10.1371/journal.pone.0020472

Růžek, D., Vancová, M., Tesařová, M., Ahantarig, A., Kopecký, J., & Grubhoffer, L. (2009). Morphological changes in human neural cells following tick-borne encephalitis virus infection. *Journal of General Virology*, *90*, 1649–1658. https://doi.org/10.1099/vir.0.010058-0

Sabouri, A. H., Marcondes, M. C., Flynn, C., Berger, M., Xiao, N., Fox, H. S., & Sarvetnick, N. E. (2014). TLR signaling controls lethal encephalitis in WNV-infected brain. *Brain Research*, *1574*, 84–95. https://doi.org/10.1016/j.brainres.2014.05.049

Schwaiger, M., & Cassinotti, P. (2003). Development of a quantitative real-time RT-PCR assay with internal control for the laboratory detection of tick borne encephalitis virus (TBEV) RNA. *Journal of Clinical Virology*, *27*, 136–145. https://doi.org/10.1016/S1386-6532(02)00168-3

Sharma, S., tenOever, B. R., Grandvaux, N., Zhou, G. P., Lin, R., & Hiscott, J. (2003). Triggering the interferon antiviral response through an IKK-related pathway. *Science*, *300*, 1148–1151. https://doi.org/10.1126/science.1081315

Shipley, J. G., Vandergaast, R., Deng, L., Mariuzza, R. A., & Fredericksen, B. L. (2012). Identification of multiple RIG-I-specific pathogen associated molecular patterns within the West Nile virus genome and antigenome. *Virology*, *432*, 232–238. https://doi.org/10.1016/j.virol.2012.06.009

Spanier, J., Lienenklaus, S., Paijo, J., Kessler, A., Borst, K., Heindorf, S., Baker, D. P., Kroger, A., Weiss, S., Detje, C. N., Staeheli, P., & Kalinke, U. (2014). Concomitant TLR/RLH signaling of radioresistant and radiosensitive cells is essential for protection against vesicular stomatitis virus infection. *Journal of Immunology*, *193*(6), 3045–3054.

Suthar, M. S., Aguirre, S., & Fernandez-Sesma, A. (2013). Innate immune sensing of flaviviruses. *PLoS Path*, *9*, e1003541. https://doi.org/10.1371/journal.ppat.1003541

Suthar, M. S., Diamond, M. S., & Gale, M., Jr. (2013). West Nile virus infection and immunity. *Nature Reviews Microbiology*, *11*, 115–128. https://doi.org/10.1038/nrmicro2950

Tegtmeyer, P.-K., Spanier, J., Borst, K., Becker, J., Riedl, A., Hirche, C., Ghita, L., Skerra, J., Baumann, K., Lienenklaus, S., Doering, M., Ruzsics, Z., & Kalinke, U. (2019). STING induces early IFN-β in the liver and constrains myeloid cell-mediated dissemination of murine cytomegalovirus. *Nature Communications*, *10*, 2830. https://doi.org/10.1038/s41467-019-10863-0

Trudler, D., Farfara, D., & Frenkel, D. (2010). Toll-like receptors expression and signaling in glia cells in neuro-amyloidogenic diseases: Towards future therapeutic application. *Mediators of Inflammation*, *2010*, 1–12.

Tsai, Y. T., Chang, S. Y., Lee, C. N., & Kao, C. L. (2009). Human TLR3 recognizes dengue virus and modulates viral replication in vitro. *Cellular Microbiology*, *11*, 604–615.

Upadhyay, A. S., Stehling, O., Panayiotou, C., Rösser, R., Lill, R., & Överby, A. K. (2017). Cellular requirements for iron-sulfur cluster insertion into the antiviral radical SAM protein viperin. *Journal of Biological Chemistry*, *292*, 13879–13889. https://doi.org/10.1074/jbc.M117.780122

Vanwalscappel, B., Tada, T., & Landau, N. R. (2018). Toll-like receptor agonist R848 blocks Zika virus replication by inducing the antiviral protein viperin. *Virology*, *522*, 199–208. https://doi.org/10.1016/j.virol.2018.07.014

Wu, M. F., Chen, S. T., Yang, A. H., Lin, W. W., Lin, Y. L., Chen, N. J., Tsai, I. S., Li, L., & Hsieh, S. L. (2013). CLEC5A is critical for dengue virus-induced inflammasome activation in human macrophages. *Blood*, *121*, 95–106. https://doi.org/10.1182/blood-2012-05-430090

Yamamoto, M., Sato, S., Hemmi, H., Hoshino, K., Kaisho, T., Sanjo, H., Takeuchi, O., Sugiyama, M., Okabe, M., Takeda, K., & Akira, S. (2003). Role of adaptor TRIF in the MyD88-independent toll-like receptor

signaling pathway. *Science*, *301*, 640–643. https://doi.org/10.1126/science.1087262

Zheng, Z., Yang, J., Jiang, X., Liu, Y., Zhang, X., Li, M., Zhang, M., Fu, M., Hu, K., Wang, H., Luo, M.-H., Gong, P., & Hu, Q. (2018). Tick-borne encephalitis virus nonstructural protein NS5 induces RANTES expression dependent on the RNA-dependent RNA polymerase activity. *Journal of Immunology*, *201*(1), 53–68.

## SUPPORTING INFORMATION

Additional Supporting Information may be found online in the Supporting Information section.

Transparent Peer Review Report

Transparent Science Questionnaire for Authors

Figure S1. Morphological analysis of untreated murine primary CNS resident cells. Primary murine neurons, astrocytes and microglia from C57BL/6 (WT) mice were mock-treated and at 12 hr post treatment, cells were immunolabelled with either anti-Tuj1 (neurons), anti-GFAP (astrocytes), or anti-Iba1 (microglia) and anti-dsRNA (J2, Scicons English and Scientific Consulting, TBEV replication foci) and counterstained with DAPI. Scale bar 20 μm

Figure S2. Verification of astrocyte identity by evaluation of astrocyte-specific transcripts. Relative expression of transcripts obtained from uninfected WT astrocytes compared with transcriptome from the total CNS, highlighting specific transcripts for astrocytes based on a previously published database (Haimon et al., 2018), (each column represents an individual sample)

Figure S3. Upon TBEV infection, MAVS-deficient astrocytes show lower induction of transcripts than WT astrocytes. (a) Comparison of total gene counts in uninfected (ctrl) and TBEV infected WT and MAVS ko astrocytes at 12 and 24 hpi. (b) Heatmaps showing relative expression of transcripts obtained from transcriptome analysis of WT and MAVS ko astrocytes either uninfected or infected for 12 and 24 hours with TBEV (each column represents an individual sample). (c) $Log_2$ fold change of significantly altered cytokine and chemokine transcripts of infected MAVS ko astrocytes relative to WT astrocytes. Cutoffs: absolute $log_2$ fold change >2

**How to cite this article:** Ghita, L., Breitkopf, V., Mulenge, F., Pavlou, A., Gern, O. L., Durán, V., Prajeeth, C. K., Kohls, M., Jung, K., Stangel, M., Steffen, I., & Kalinke, U. (2021). Sequential MAVS- and MyD88/TRIF-signaling triggers anti-viral responses of tick-borne encephalitis virus-infected murine astrocytes. *Journal of Neuroscience Research*, 99, 2478–2492. https://doi.org/10.1002/jnr.24923